

## Failure of circular tunnel in saturated soil subjected to internal blast loading

Yuzhen Han<sup>1a</sup> and Huabei Liu<sup>\*2</sup>

<sup>1</sup> Beijing Urban Construction Design & Development Group Co., Limited,  
No. 5, Fuchengmen Beidajie, Xicheng District, Beijing 100037, China

<sup>2</sup> School of Civil Engineering and Mechanics, Huazhong University of Science and Technology,  
1037 Luoyu Road, Wuhan, Hubei 430074, China

(Received November 04, 2015, Revised April 28, 2016, Accepted May 13, 2016)

**Abstract.** Explosions inside transportation tunnels might result in failure of tunnel structures. This study investigated the failure mechanisms of circular cast-iron tunnels in saturated soil subjected to medium internal blast loading. This issue is crucial to tunnel safety as many transportation tunnels run through saturated soils. At the same time blast loading on saturated soils may induce residual excess pore pressure, which may result in soil liquefaction. A series of numerical simulations were carried out using Finite Element program LS-DYNA. The effect of soil liquefaction was simulated by the Federal Highway soil model. It was found that the failure modes of tunnel lining were differed with different levels of blast loading. The damage and failure of the tunnel lining was progressive in nature and they occurred mainly during lining vibration when the main event of blast loading was over. Soil liquefaction may lead to more severe failure of tunnel lining. Soil deformation and soil liquefaction were determined by the coupling effects of lining damage, lining vibration, and blast loading. The damage of tunnel lining was a result of internal blast loading as well as dynamic interaction between tunnel lining and saturated soil, and stress concentration induced by a ventilation shaft connected to the tunnel might result in more severe lining damage.

**Keywords:** blast loading; cast-iron lining; failure modes; soil-lining interaction; soil liquefaction

---

### 1. Introduction

Explosions inside transportation tunnels might result in immediate casualties; and the subsequent failure of tunnel structures could further lead to significant socioeconomic losses. Technology should therefore be developed and validated to address the need of tunnel safety. This study aims to facilitating this objective through fundamental investigation on failure mechanisms of circular tunnels in saturated soil subjected to medium internal blast loading.

This issue is crucial to tunnel safety considering that many transportation tunnels run through saturated soils. Blast loading of saturated soils induces drastic changes of compressive strain and excess pore pressure, and the residue of excess pore pressure will reduce effective stress and may result in soil liquefaction (Fragaszy and Voss 1986, Veyra and Charlie 1990, Ashford *et al.* 2004).

---

\*Corresponding author, Professor, E-mail: [hbliu@hust.edu.cn](mailto:hbliu@hust.edu.cn)

<sup>a</sup> Ph.D., E-mail: [hanyuzhen815@gmail.com](mailto:hanyuzhen815@gmail.com)

The developments of pore water pressure, effective stress and soil deformation interact with the tunnel lining and internal blast pressure, complicating the tunnel responses and damages (Chou *et al.* 2001, Liu and Song 2006, Feldgun *et al.* 2008, Liu 2009, 2012).

Few studies can be found in the literature on the responses of civilian underground structures subjected to internal blast loading. Choi *et al.* (2006), through analysis of coupled air-solid interaction, found that the blast pressure on tunnel lining was not the same as the CONWEP normally reflected pressure on rigid surface (UFC 3-340-02 2008). Liu and Nezili (2016) carried out a centrifuge test on the blast response of a buried pipe under internal blast loading and found that projectiles from the model explosive severely damaged the pipe. Feldgun *et al.* (2008) investigated the two-dimensional response of a lined tunnel subjected to idealized blast loading from a line charge. He *et al.* (2011) investigated the dynamic response of a subway station under internal blast loading. Recently, Chakraborty *et al.* (2014) compared the response of tunnel with different lining materials under simplified internal blast loading of small magnitude. On a related subject, some studies can be found on the propagation of blast waves in the ground and their effects on underground structures, but the findings cannot be applied to the problem of interest in this study (Lu *et al.* 2005, Koneshwaran *et al.* 2015, De 2012).

Most of the existing studies did not pay enough attention to the importance of saturated ground – tunnel interaction. Liu (2009, 2012) established a Finite Element procedure to capture the dynamic and nonlinear response of the ground-tunnel system subjected to simplified internal blast loading, in which the importance of dynamic soil-structure interaction was identified. However, the Finite Element models in Liu (2009, 2012) did not consider the effect of soil liquefaction after blast loading, and the simplified loading did not properly take into account the coupled interaction between air and solid. They also did not model the propagation of blast wave in the tunnel. These problems hindered the full understanding of failure mechanisms.

In this study, single-track circular subway tunnels in saturated dense soils and lined by low-grade gray cast-iron lining, which are common in the century-old subway systems in New York City and London, were investigated for their failure mechanisms under internal blast loading. Finite Element procedure using LS-DYNA (2012a, b) was employed to analyze the tunnel responses. Explosives ranging from 50 kg TNT to 200 kg TNT were assumed to be ignited at the center of the tunnels. Different failure modes were identified under different scenarios of blast loading, and the influences of lining and soil parameters were studied. To the writers' knowledge, the failure modes and the influence of soil liquefaction revealed by this study have never been presented before.

## 2. Finite element procedure

The analyses in this study involved the following Finite Element simulations: blast loading, interaction between air pressure and tunnel lining, lining materials, saturated soil, and soil-lining interactions.

The blast loading and air-lining interaction were modeled using a new blast loading scheme (Load\_Blast\_Enhanced) available in LS-DYNA (Han and Liu 2015). Only the air immediately surrounding the tunnel lining is modeled by Eulerian air elements. Time histories of incident blast pressure are applied to a layer of special Eulerian elements, which is herein referred to as the ambient layer (Han and Liu 2015). The ambient layer faces the explosive charge and acts as a source for the adjoining air elements. Time histories of incident blast pressure applied to the ambient layer are derived from CONWEP. The blast wave then propagates through the air domain

and eventually interacts with the tunnel lining through Arbitrary Lagrange Eulerian (ALE) coupling scheme. The loading on the structure due to wave reflection and superposition can then be captured by the air elements. The application and validity of this numerical approach for simulating the effect of blast loading on structures have been discussed by Han and Liu (2015).

The air in all the numerical simulations was modeled using linear 3D solid elements in LS-DYNA. The elements were 8-node hexahedron elements integrated using 8-point Gaussian method. The air was assumed to be ideal gas and modeled using the MAT\_NULL material model, the equation of state of which is given as

$$p = (\gamma - 1) \frac{\rho}{\rho_0} E_0 \quad (1)$$

Here  $\gamma$  is the ratio of specific heat and was assumed as 1.4 according to previous numerical experiences (Han and Liu 2015).  $\rho_0$  is the initial density of air.  $E_0$  was given a value of 0.25 MPa assuming an initial air temperature of 20°C.

An isotropic elastoplastic model (MAT 124 Plasticity Compression Tension) in LS-DYNA was used to simulate the grey cast-iron tunnel lining. In this model curves of uniaxial yielding stress versus plastic strain can be defined for compression and tension, respectively. Thus this model can be employed to simulate cast-iron, the compressive strength of which is much higher than its tensile strength. Rupture of cast-iron can also be simulated by deleting the element when the tensile strength is mobilized. The model is briefly introduced in Appendix A. Rate effect can be taken into account by the model but it was not employed in this study due to lack of testing data. Instead, a parametric study with different strengths and moduli of cast-iron was carried out to investigate their influences on tunnel response.

Federal Highway (FHWA) soil model (Lewis 2004) was employed to model the saturated soil (MAT 147 in LS-DYNA) (Jayasinghe *et al.* 2013, 2014). Considering the nature of rapid blast loading, undrained response of saturated soil was assumed in this study. FHWA soil model is a modified Drucker-Prager plasticity model and is capable of simulating the pre-peak strain hardening and post-peak strain softening of soils. It can also reproduce the residual pore water pressure under compressive loading and unloading, hence the onset of blast-induced soil liquefaction may be captured. However, the model assumes associated flow rule, which tends to over-estimate the dilation of soil after yielding. As a result, the pore water pressure may be underestimated when the liquefied soil undergoes large shear deformation. Similar to the cast-iron model, rate effect can be simulated by the FHWA soil model, but it was not considered in this study due to lack of test data. Instead, soil strength and soil modulus were varied to investigate their influences. The constitutive model is briefly introduced in Appendix B.

Thin-layer elements are used to simulate the interface between soil and tunnel. The concept has been employed extensively in analyses of soil-structure interactions (Desai *et al.* 1984). Ordinary solid elements was used to simulate the interfaces, but the thickness was about 0.01~0.1 of the longer dimension. Material model of the thin-layer elements was the same as that of the soil, but with reduced strength and shear modulus.

### 3. Finite element model

As shown in Fig. 1, the Finite Element model consists of soil, soil-tunnel interface, tunnel lining, air and ambient layer. Due to symmetry, only one quarter of the soil-tunnel system was

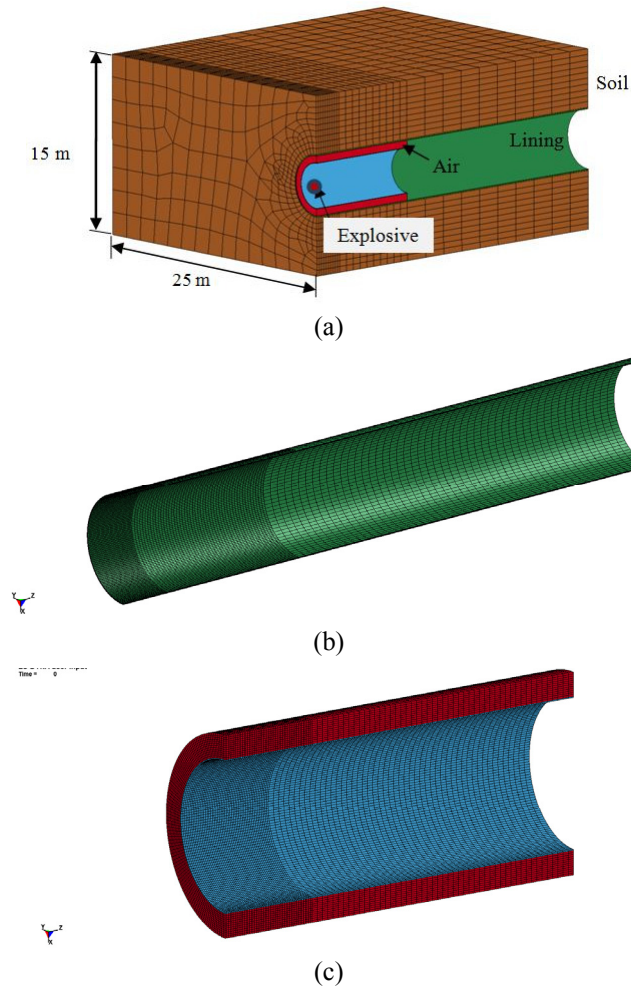


Fig. 1 Finite Element model: (a) Soil mesh (length in prototype scale); (b) Mesh of tunnel lining; (c) Mesh of air domain

simulated. The prototype model is based on single-track subway tunnels in New York City. The diameter of the tunnel was assumed to be 5 m and the tunnel was buried 5 m below the ground surface. The soil ground was assumed to be saturated and the thickness of dense saturated soil layer was assumed to be 15 m, the base of which was stiff bed rock and fixed in the Finite Element model. The lining thickness was assumed to be 6 cm based on the parameters of cast-iron subway tunnels in New York City. The Finite Element model was fixed at the base and roller boundaries were applied to the four sides. The soil, the thin-layer interface and the tunnel lining were all modeled using 8-node hexahedron solid elements.

The tunnel lining was modeled by 3 layers of solid elements, which have different element sizes along the longitudinal direction, as shown in Fig. 1(b). In the prototype model, the element length was 5 cm in the first 250 cm section, 15 cm in the next 750 cm section, and 40 cm in the remaining lining model. These Finite Element parameters have been determined by trial analyses. With smaller element sizes, the responses of the tunnel were basically identical.

The Finite Element size and thickness of the air domain in the tunnel were determined by two steps. Firstly, the reflected pressure and specific impulse on a rigid surface were analyzed using different sizes of air elements. The results were then compared to the curves in UFC 3-340-02 (2008), focusing on the scaled distance  $Z$  of interest ( $Z = R/\sqrt[3]{W}$ , in which  $R$  is the standoff distance and  $W$  is the weight of TNT). In this study, the amount of TNT of interest ranged from 50 kg to 200 kg. Corresponding to a tunnel radius of 2.5 m, the scaled distance of interest was larger than  $0.427 \text{ m/kg}^{1/3}$ . The element size was thus determined when the peak reflected pressure and specific impulse were very close to the ones in UFC 3-340-02 (2008). In the next step, the thickness of air domain was determined by parametric analyses. Different thicknesses of air domain were investigated inside a rigid tunnel having a diameter  $D = 5 \text{ m}$ . 200 kg of TNT was assumed to be ignited at the center of the tunnel. The result shows that the peak blast pressure was basically not affected by the air thickness, while the specific impulse decreased with an increase in the thickness. The specific impulse tended to converge when the thickness was larger than 30% of the tunnel radius. With a thickness of 24% tunnel radius, the specific impulse of the blast pressure on the lining was conservative to some extent. Since in the blast-resistant design of structures, it is of common practice to apply a factor of safety to the blast loading (UFC 3-340-02 2008), this thickness was employed in this study.

The air domain and ambient layer was modeled as shown in Fig. 1(c). The length in the longitudinal direction was only 1/3 of the model tunnel. Analysis consisting of full-length of air in the tunnel was also carried out for comparison. The results showed that the air domain as shown in Fig. 1(c) was sufficient. Here the air domain and ambient layer were modeled with the same material model parameters for the air elements. The prototype thickness of the air domain was 60 cm, with the thickness of the air element being 5 cm, and the thickness of the ambient layer element was 2.5 cm. The length of the air elements was the same as that of the adjacent lining element.

The dense saturated soil was modeled by FHWA Soil Model. Most of the default parameters in LS-DYNA were employed in this study, which were calibrated by the model developer for dense granular soil with cohesive fines (Lewis 2004). However, the parameter  $K_{sk}$  that controls the development of pore water pressure was assumed to be 175 MPa in the base case. According to Lewis (2004), this value of  $K_{sk}$  corresponds to a Skempton parameter  $B = 0.87$ . It is noted that much smaller  $B$  value for saturated soil was observed in Fragaszy and Voss (1986) when the soil was subjected to large compressive loading. The influence of  $K_{sk}$  on soil liquefaction and tunnel response was also investigated in the parametric study. Table 1 shows the model parameters. The thin-layer elements between soil and lining were also modeled by FHWA soil model, but their shear modulus and shear strength were assumed as two thirds of those of soil. Smaller element size of soil was employed close to the tunnel, so that more accurate response of the saturated soil can be captured in the analysis.

Table 1 Parameters of FHWA soil model

Bulk Modulus $K$ (MPa)	Shear Modulus $G$ (Mpa)	Saturated unit weight (MN/m <sup>3</sup> )	$\phi_{\max}$ (°)	$c$ (MPa)	ahyp
465	186	0.023	38	0.0062	1.00E-07
$e$	$A_n$	$E_t$	$K_{sk}$ (MPa)	$\phi_{\text{int}}$ (°)	
0.7	0	10	175	0	

The density of cast iron lining was  $7.89 \text{ g/cm}^3$ . Its Young's modulus was assumed to be 100 GPa based on the value of low-grade grey cast-iron, with a Poisson's ratio of 0.27 (Davis 1996). In the tensile direction, the failure stress is 150 MPa when the tensile strain reached 0.004, while in the compressive direction the yield stress was 600 MPa. The damping ratio of the cast-iron was assumed to be 2% in the base case. The strength, Young's modulus, and damping ratio of the lining material were also varied in the parametric study to investigate their influence.

#### 4. Results

The blast effects caused by three different amounts of explosive, which were assumed to be ignited at the center of the tunnel, were investigated in this study. Fig. 2 shows the incident blast pressures in the ambient layers that are closest to the explosives. It is noted that the arriving time was different with different magnitudes of explosion.

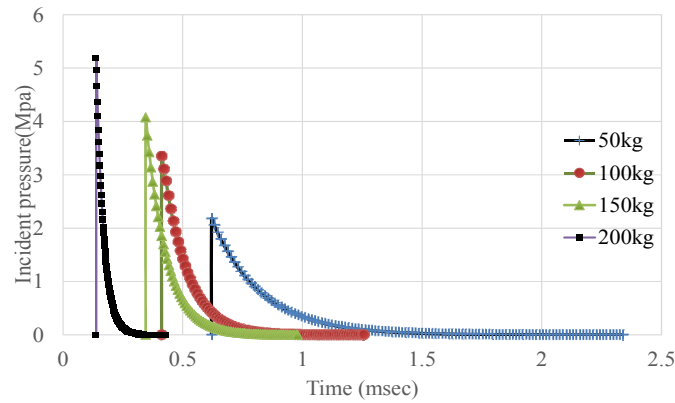


Fig. 2 Incident pressures in the ambient layer closest to the explosive

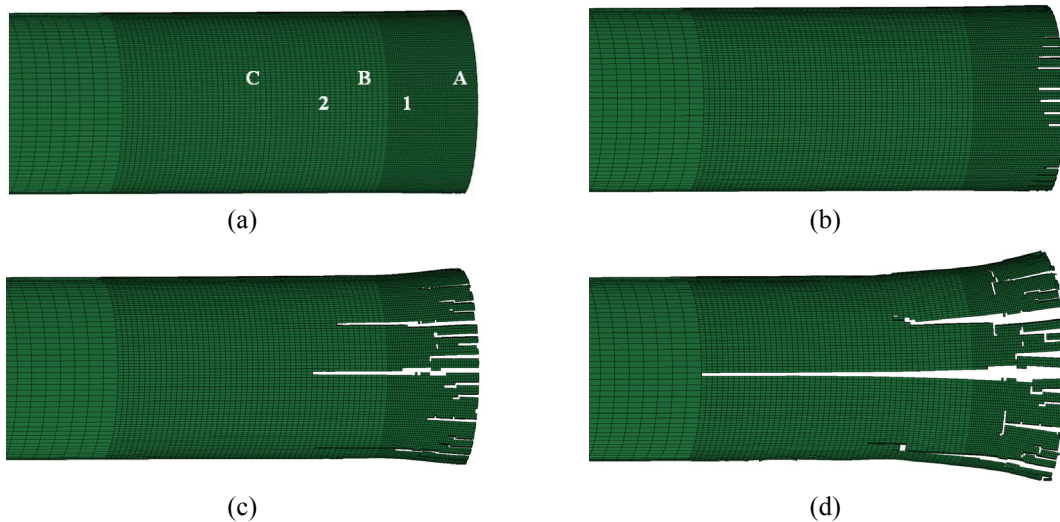


Fig. 3 Lining failure at different moments after explosion (200 kg TNT; deformation enlarged 10 times): (a)  $t = 1.2 \text{ ms}$ ; (b)  $t = 1.35 \text{ ms}$ ; (c)  $t = 4.5 \text{ ms}$ ; (d)  $t = 9.42 \text{ ms}$

#### 4.1 Simulation Results with 200 kg TNT

In this case, the analysis stopped at 9.5 ms after explosion, due to extensive failure in the soil and lining.

##### 4.1.1 Lining failure

The lining failures at different moments after explosion are shown in Fig. 3. The failure occurred first in the lining close to the explosive due to large hoop stress in tension. It then propagated to the adjacent section, and extended as far as 10 m away from the cross-section where the explosive was located. Lining fracture began to appear at 1.125 ms, but the main event of blast wave was almost over at this instant, as shown in Fig. 4.

The accelerations at two locations in the lining are shown in Fig. 5. Positive values herein represent the expansion of tunnel lining under blast loading. The lining experienced a large acceleration, and the acceleration close to the explosive was higher than that farther away from it. The tunnel basically expanded under the large blast loading, as can be seen from the deformed shape in Fig. 3.

The main influence of blast loading occurred in the soil not far away from the explosive. Fig. 6 shows the distributions of effective shear strain ( $\epsilon_s = \int \sqrt{\frac{2}{3} de_{ij} de_{ij}}$ ) inside the soil at two instants. The maximum shear strain in the soil close to the blast loading was 23%. In addition, although not clearly demonstrated herein, some soil elements were penetrated by the fractured tunnel lining.

Upon unloading in the soil after blast loading, residual pore water pressure existed and at some

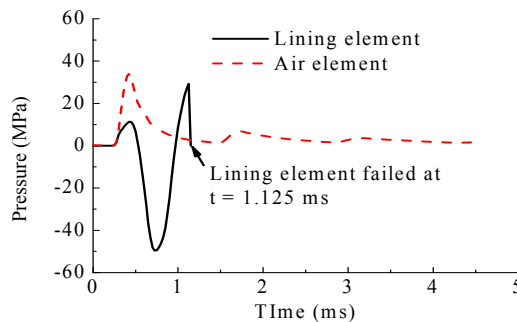


Fig. 4 Pressures in a lining element and the adjacent air element close to the explosive

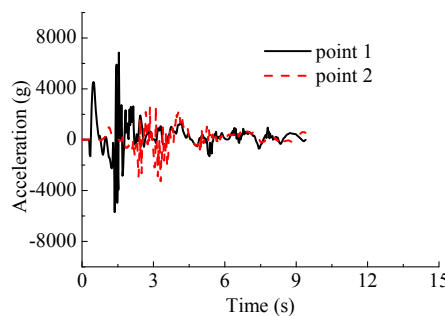


Fig. 5 Accelerations at two locations on the lining (point 1 and point 2 are illustrated in Fig. 3(a))

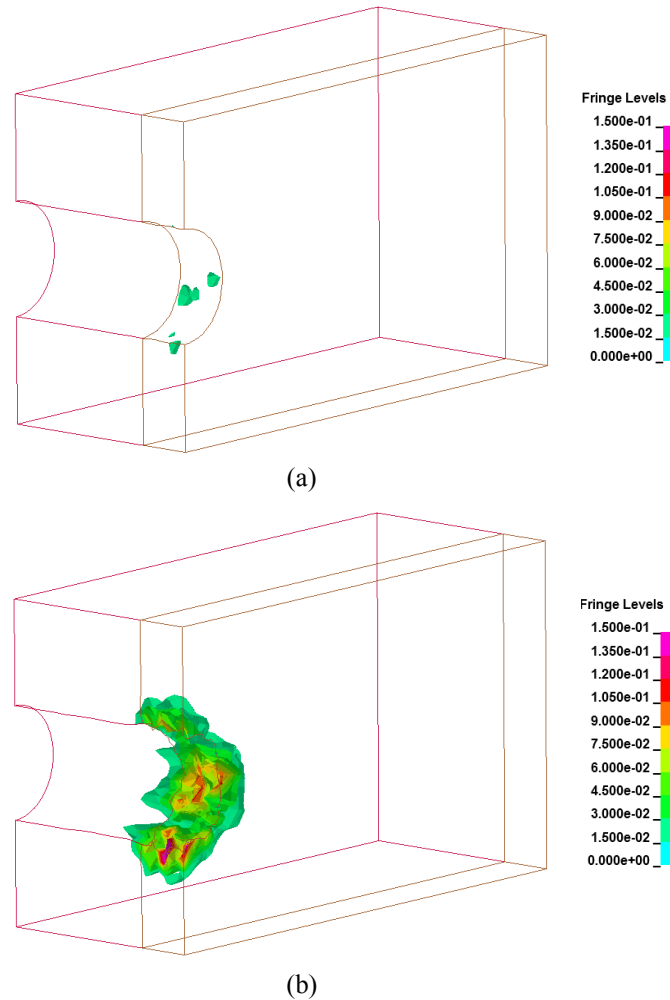


Fig. 6 Distributions of effective shear strains in the soil (a)  $t = 6.5$  ms; (b)  $t = 9.42$  ms

locations the mean effective stress reduced to zero, indicating soil liquefaction. Fig. 7 shows the liquefied soil elements at the end of analysis. Liquefaction was concentrated in the soil near the explosive. It should be pointed out that Fig. 7 did not represent all the liquefied soil during the whole analysis. The constitutive model of soil assumes associated flow rule and the model soil dilated considerably when it started yielding. This unrealistic dilation would result in reduction of pore water pressure and increase of effective stress. Due to this defect in the constitutive model, a soil element liquefied after the end of blast pressure, but the liquefaction disappeared at the same location when the soil element started yielding and dilating due to small effective stress.

## 4.2 Simulation Results with 100 kg TNT

### 4.2.1 Lining failure

The lining failure was not extensive in this case, as shown in Fig. 8 together with the distributions of plastic strains. Lining fracture emerged at about 1.5 ms after explosion at the top of

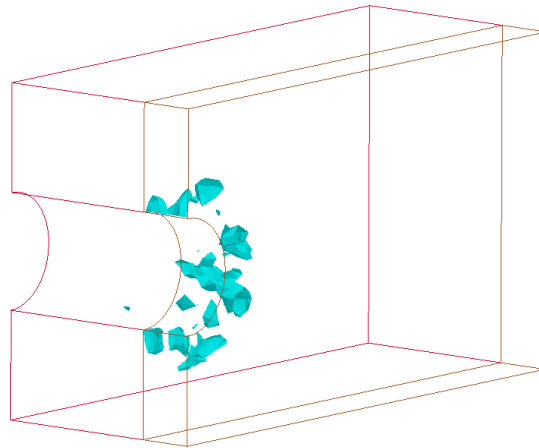


Fig. 7 Distribution of liquefied soil at  $t = 9.42$  ms (dark color indicates soil liquefaction)

the tunnel; further fracture occurred about 8 ms afterwards at the bottom. In addition, lining rupture did not occur in the section closest to the explosive.

#### 4.2.2 Lining acceleration and displacement

The tunnel experienced large vibration under blast loading as can be seen from the deformed shape in Fig. 8. Fig. 9 shows the time histories of accelerations and displacements at two locations. It can be seen that the accelerations were much larger than the 200 kg case, and the acceleration at point 2, which was farther away from the explosive, was larger. Apparent phase-lag in the motions of the lining at different locations can also be clearly witnessed in Figs. 8 and 9.

Since lining damage was much smaller in this case than in the 200 kg TNT case, lining vibration was more significant, although the blast loading was smaller. It also appears that the lining fracture was caused by the phase-lag of vibration, as can be seen in Fig. 8 and Fig. 9. The directions and magnitudes of lining displacements and accelerations at different locations were different, resulting in large tensile stress in the axial direction at certain location that caused lining

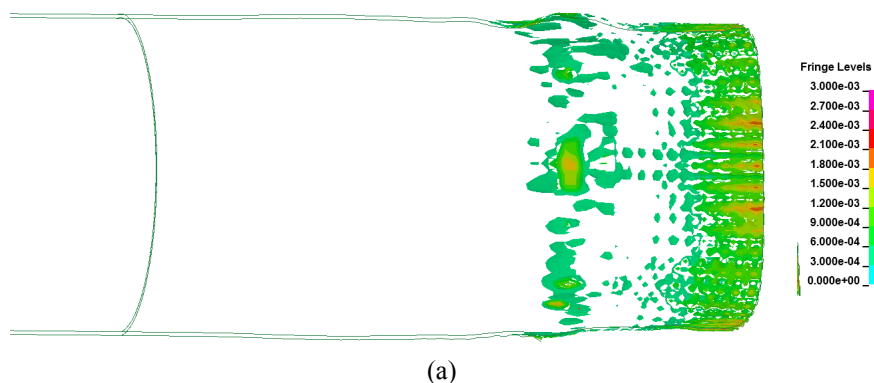


Fig. 8 Lining failure at different moments after explosion (100 kg TNT; deformation enlarged 20 times): (a)  $t = 7.5$  ms; (b)  $t = 12.5$  ms; (c)  $t = 15$  ms

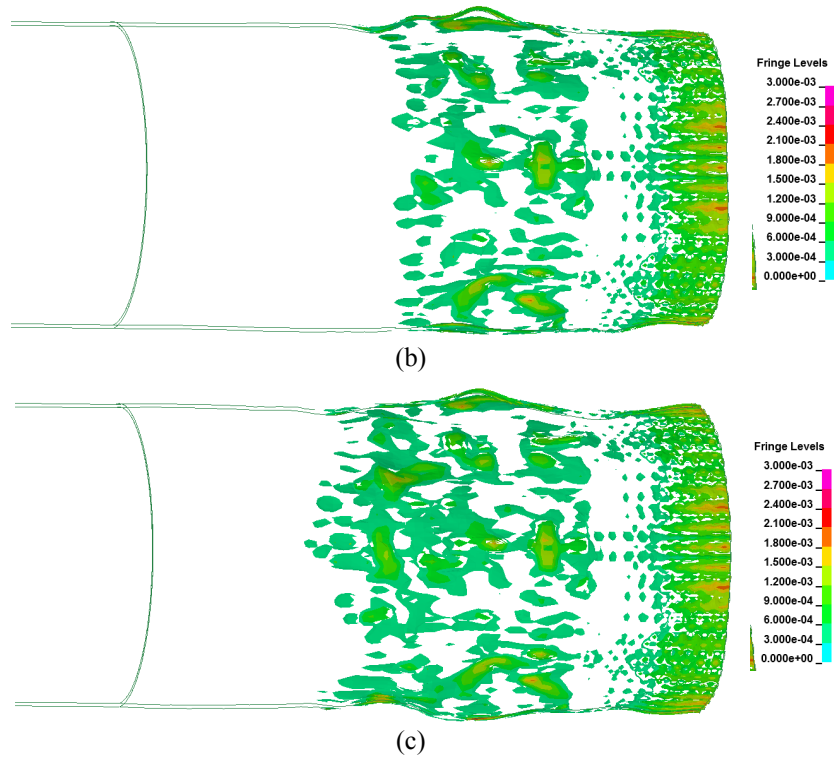


Fig. 8 Continued

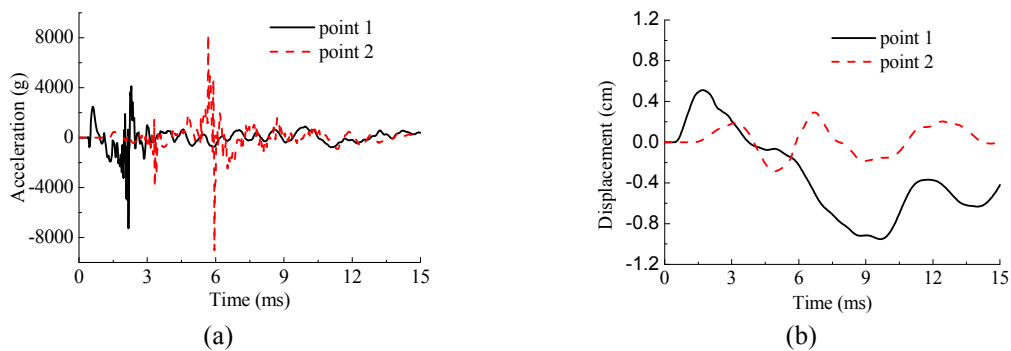


Fig. 9 Time histories of accelerations and displacements at two locations (100 kg TNT; point 1 and point 2 are illustrated in Fig. 3(a))

rupture. This phase lag was mostly initiated by the different moments of blast loading on the lining. This phenomenon cannot be captured by the simplified blast loading in Liu (2009, 2012).

#### 4.2.3 Soil response

Due to the large vibration of tunnel lining, much blast energy propagated into the soil, resulting in large deformation and extensive liquefaction in the soil, as shown in Fig. 10. The soil began to liquefy at about 4 ms and the liquefaction extended to the top and bottom of the soil layer.

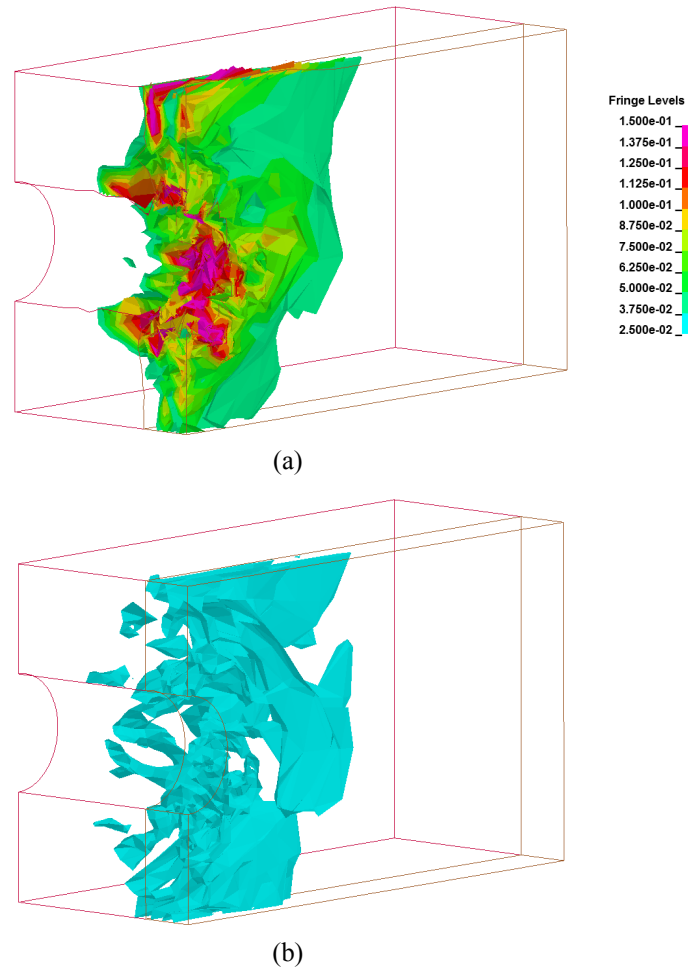


Fig. 10 Distributions of shear strain and soil liquefaction at  $t = 15$  ms (100 kg TNT): (a) effective shear strain; (b) soil liquefaction (dark color indicates soil liquefaction)

#### 4.3 Simulation Results with 50 kg TNT

In this case, the tunnel lining did not fracture, but some lining elements on the outside surface near the explosion failed. The lining vibration assumes similar characteristic as that of the 100 kg TNT case, although the magnitudes of accelerations were slightly smaller. Lining damage was caused by lining vibration, which resulted in large tensile stress in the axial direction. The acceleration in the shrinking direction was actually larger, which explains the damaged elements on the outside surface of the tunnel. The shear deformation in the soil was also large in this case, but soil liquefaction was not as extensive as in the 100 kg TNT case.

#### 4.4 Parametric study

A Parametric study was carried out to understand the influences of lining and soil parameters. These parameters consist of lining strength and stiffness, lining damping, soil bulk modulus and

strength, and liquefaction susceptibility of soil. The influence of a ventilation shaft on the tunnel was also investigated. 100 kg TNT was assumed to explode at the center of the tunnel in the parametric study, and except the parameter of interest, the others were maintained the same as the base case in the last section. In the following presentation, the focus is placed on the failure mechanisms of the lining. The extents of soil liquefaction are only described by texts without figures to save space.

#### 4.4.1 Lining strength and stiffness

In this series of simulation, the strength and stiffness of lining were varied proportionally in order to model the possible effects of temperature increase and large loading rate. As shown in Fig. 11, the damage of tunnel lining was clearly dependent on these two parameters. When the strength and stiffness were increased to 110% of the base-case values, there was no fracture in the lining; and the strength and stiffness were reduced to 90%, the extent of failure and damage mode were basically the same as the ones with the original strength. However when the scale factor of strength and stiffness was further reduced, rupture firstly appeared in the lining close to the explosive, and then propagated to farther distance due to lining vibration.

Soil response was smaller with smaller strength and stiffness of lining in the investigated range. This is consistent with the finding in last section. There was extensive fracture in the lining with low strength and stiffness of tunnel lining, and only a small portion of blast energy propagated into the soil, so that the soil response was smaller.

#### 4.4.2 Lining damping

In this study, tunnel lining was assumed to be continuous, while in reality it is fabricated from lining segments connected by bolts and joints. The joint and the adjacent rubber for seepage

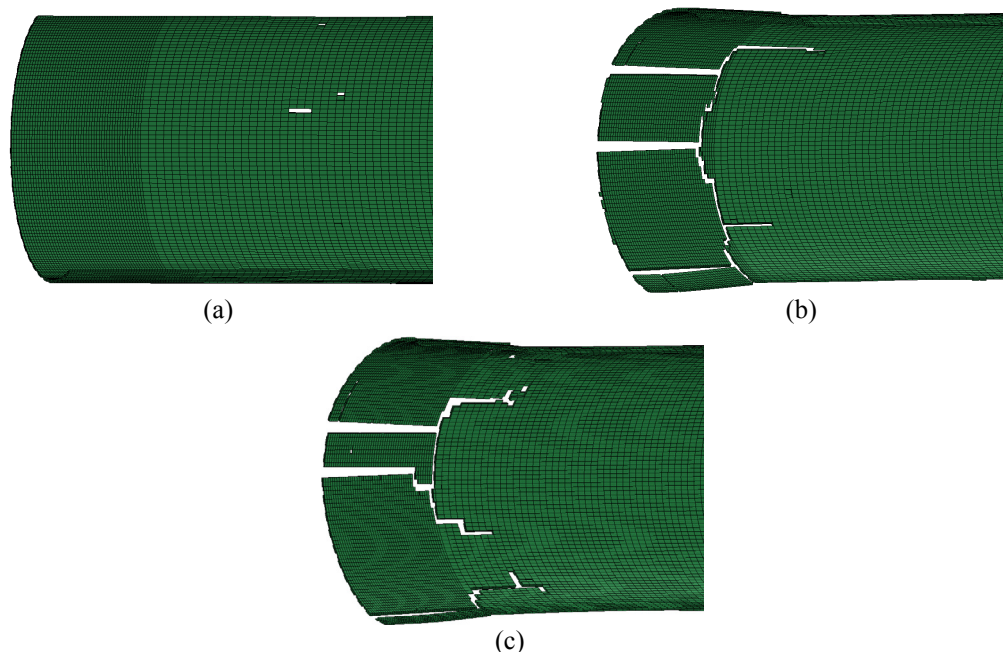


Fig. 11 Effects of lining strength and stiffness on lining failure: (a) strength and stiffness ratio = 90%; (b) strength and stiffness ratio = 80%; (c) strength and stiffness ratio = 70%

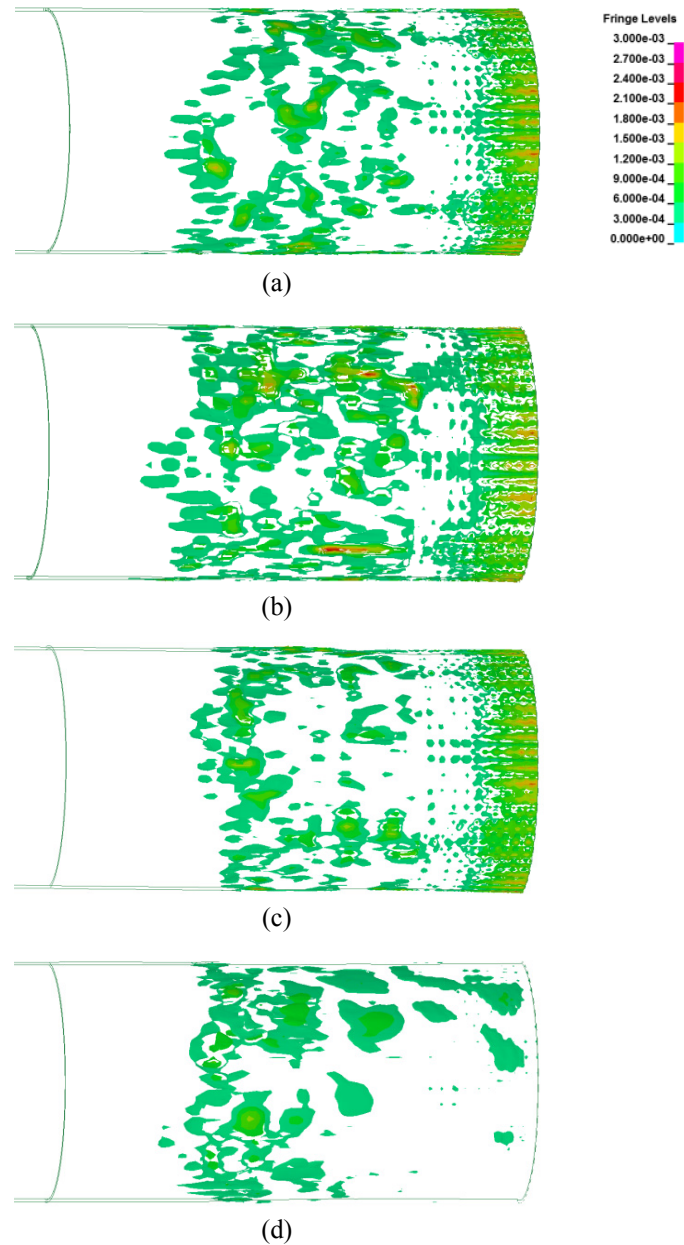


Fig. 12 Distributions of effective plastic strain in the lining: (a) damping ratio = 0%; (b) damping ratio = 2%; (c) damping ratio = 5%; (d) damping ratio = 7.5%

control may increase the lining damping. The influence of lining damping was therefore investigated. The stiffness damping ratio was assumed to be 0%, 2%, 5% and 7.5% while all other parameters remained the same.

There was some fracture in the lining when the damping ratios were 0% and 2%, but it disappeared when the damping ratio increased. The lining deformation was also much smaller with

larger damping ratio, as shown in Fig. 12. Both the soil deformation and soil liquefaction also reduced with an increase in the lining damping.

#### 4.4.3 Bulk modulus and shear strength of saturated soil

The compressibility of saturated soil under large compressive loading is determined by the compressibility of pore water and soil particles (Fragaszy and Voss 1986). Particularly, air bubbles in the pore water may considerably affect the soil compressibility. At the same time, rapid loading rate would increase the soil stiffness and soil strength (Farr 1990). Consequently, the simulation analyses were carried out with larger bulk modulus and shear strength of soil. Two bulk moduli, 600 MPa and 800 MPa, were investigated with the original friction angle of soil ( $\phi = 38^\circ$ ), and three additional friction angles,  $41.8^\circ$ ,  $45.6^\circ$ , and  $49.4^\circ$  were analyzed for their influences with the original bulk modulus of soil ( $K = 465$  MPa).

There was no lining fracture with larger bulk modulus of soil, and the lining deformation was also smaller, as can be seen in Fig. 13. Lining deformation of the base case ( $K = 465$  MPa) is shown in Fig. 12(b). The soil deformation and soil liquefaction was also considerably smaller than those of the base case. In contrast, in the investigated range, soil strength only slightly affected the response of the soil-tunnel system, the results of which are not presented herein to save space. This finding is consistent with the previous one by the corresponding author (Liu 2012).

#### 4.4.4 Liquefaction susceptibility of saturated soil

Liquefaction susceptibility of saturated soil under blast loading is determined by particle crushability of soil and compressibility of pore water (Fragaszy and Voss 1986). In the numerical simulations of this study, it was governed by the parameter  $K_{sk}$ , which determines the build-up of pore water pressure as a function of the volumetric strain of soil. A series of simulations with different values of  $K_{sk}$  were conducted to investigate its influence.

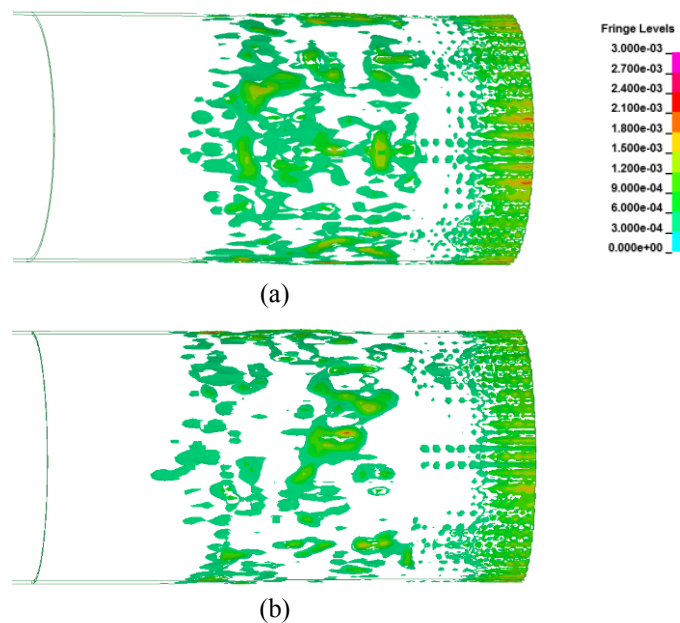


Fig. 13 Distributions of effective plastic strain in the lining: (a)  $K = 600$  MPa; (b)  $K = 800$  MPa

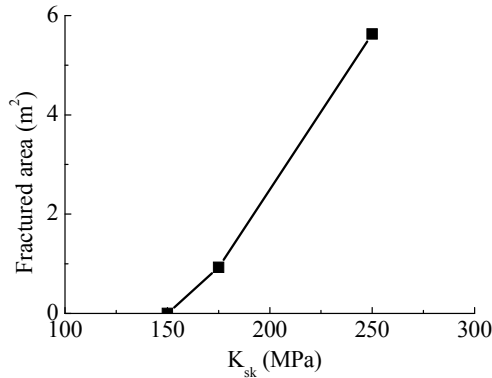


Fig. 14 Effect of liquefaction susceptibility on lining failure

As expected, soil deformation and liquefaction were directly affected by the liquefaction susceptibility of saturated soil. Both the shear deformation and liquefaction of soil increased significantly with an increase in the liquefaction susceptibility. The increase of soil deformation reduced the confinement and support on the tunnel and resulted in much more severe damage in the lining, as can be seen in Fig. 14.

4.4.5 Influence of ventilation shaft

The existence of ventilation shaft in close proximity of blast loading would modify the pattern of blast pressure propagation and change the response of the tunnel lining. Simulations were therefore conducted with ventilation a ventilation shaft to investigate its influence on the failure modes due to blast loading. As shown in Fig. 14(a), the ventilation shaft was assumed to be of 1 m × 1 m in size. Blast loading due to 50 kg TNT or 100 kg TNT was assumed to occur next to the shaft at the center of the tunnel.

Fig. 15(b) shows the peak pressures at different incident angles of blast loading from 100 kg TNT on the lining close to the ventilation shaft. The peak pressure on the lining reduced significantly in the area close to the ventilation shaft, but it can be seen that the ventilation shaft

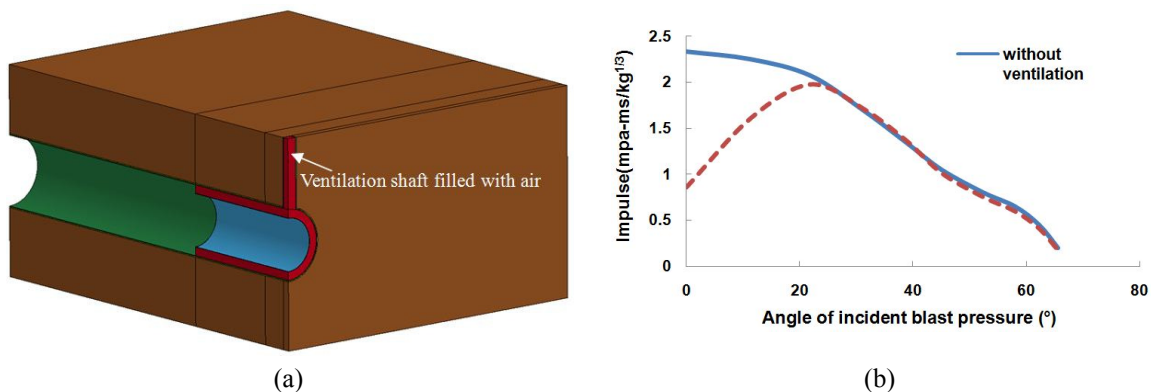


Fig. 15 Influence of ventilation shaft: (a) Finite Element model; (b) peak blast pressure next to the shaft; (c) failure modes of tunnel lining (deformation enlarged 20 times); (d) acceleration at point 1 (point 1 is illustrated in Fig. 3(a))

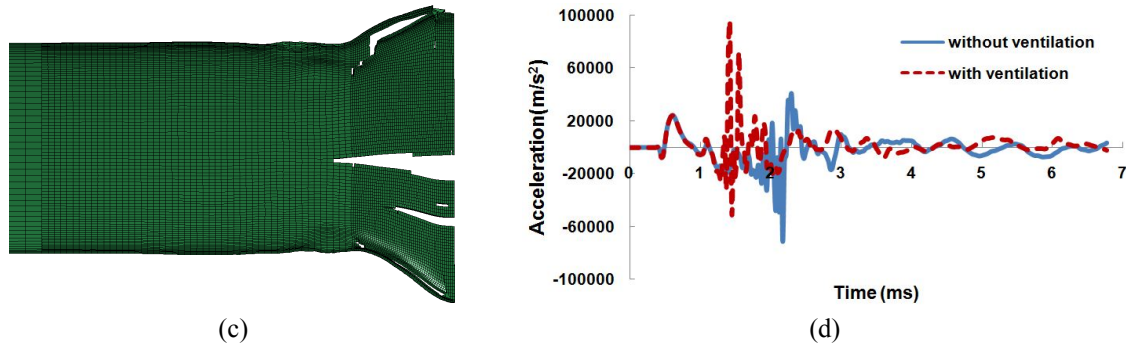


Fig. 15 Continued

reduced the blast pressure only in its close proximity. The same conclusion also applies to the specific impulse.

However, with 100 kg TNT, the lining had more extensive damage with the ventilation shaft, as shown in Fig. 15(c). The lining damage without ventilation shaft is shown in Fig. 8. Failure was initiated in the lining next to the corner of the ventilation shaft. It then became more severe with lining vibration. Fig. 15(d) shows the comparison lining accelerations at point 1 (Fig. 3(a)). Apparently, the acceleration was higher with the ventilation shaft. It can be seen that the ventilation shaft investigated herein modified the vibration characteristics of the lining. It also led to stress concentration in the lining. These two factors contributed to the more severe damage shown in Fig. 15(c).

With 50 kg TNT, the lining did not rupture, and the damage at the outside surface of the lining was also smaller with the ventilation shaft. The figures are not presented herein due to space limitation.

## 5. Discussions

As discussed in the session of Finite Element model, the air domain inside the tunnel employed in this study resulted in conservative blast loading on the lining. However, since a range of explosive charge was investigated, it is believed that the failure mechanisms identified in this study apply to the actual cases.

The Finite Element models assumed continuous tunnel lining for the sake of simplicity. It is understood that the joints between lining segments would modify the tunnel response. From the parametric study, it can be seen that the changes of lining stiffness and lining damping affected the lining damage. It is not known at present whether the joints would modify the propagation of lining rupture, which is a subject that deserves further investigation.

The excess water pressure generated in the FHWA soil material model was not 100% accurate after the soil liquefied and underwent large shear deformation. Unrealistic dilation of model soil with large shear deformation led to unrealistic increase of effective stress and shear strength. The tunnels might have experienced more severe damage due to soil liquefaction, but it could not be reproduced in this study. More sophisticated constitutive model may be necessary to duplicate this behavior (Wang *et al.* 2008, Xu and Zhang 2015).

Finally, this study was focused on the failure mechanisms due to internal blast pressure, but

projectiles from the explosion may also considerably damage the tunnel lining (Liu and Nezili 2016).

## 6. Conclusions

A series of numerical simulations were carried out in this study to investigate the failure mechanisms of circular tunnels in saturated soils subjected to medium internal blast loading. Numerical procedure using Finite Element program LS-DYNA that can model air blast, fluid-solid interaction, material damage and soil-structure interaction were used to carry out the simulations. The soil was simulated by the FHWA soil model, which has been shown to be capable of modeling saturated soil (Jayasinghe *et al.* 2013, 2014). A new coupling method was used to study the process of blast wave propagation in the air domain inside the tunnel. Extensive parametric studies were carried out to understand the failure and damage of cast-iron subway tunnels under internal blast loading and to shed light on their protection by structural and geotechnical measures. Based on extensive numerical simulations, the following conclusions can be obtained:

- (1) The failure modes of tunnel lining differed with different levels of blast loading. With relatively large blast loading, severe rupture first appeared in the lining close to the explosive, and then propagated to farther distance due to lining vibration. The failure was governed by the large hoop stress in the lining. When the blast loading were reduced to certain extent, lining fracture occurred at some distance away from the explosive, caused by the phase lag of lining vibration that resulted in large tensile stress in the axial direction. This phase lag was mostly initiated by the different moments of blast loading on the lining. Overall the damage and failure of the tunnel lining was progressive in nature. The damage and failure occurred mainly during lining vibration when the main event of blast loading was over.
- (2) Soil deformation and soil liquefaction were determined by the coupling effects of lining damage, lining vibration, and blast loading. With extensive lining fracture, only a small portion of blast energy propagated into the soil, and the extent of soil liquefaction was actually smaller. Soil liquefaction may lead to more severe failure of tunnel lining.
- (3) The numerical simulations showed that damage of tunnel lining was a result of internal blast loading as well as dynamic interaction between tunnel lining and saturated soil. Augmenting soil stiffness by certain soil reinforcement technique, increasing overburden stress of the surrounding soil without significantly increasing static lining stress, and enhancing lining damping through structural measures at its joints, may be adopted to reduce the vulnerability of a tunnel subjected to internal blast loading.

Explosion close to ventilation shafts would reduce the blast pressure on the lining, but might not alleviate lining damage due to the reduction of lining integrity and stress concentration.

## References

- Ashford, S.A., Rollins, K.M. and Lane, J.D. (2004), "Blast-induced liquefaction for full-scale foundation testing", *J. Geotech. Geoenviron. Eng., ASCE*, **130**(8), 798-806.
- Chakraborty, T., Larcher, M. and Gebbeke, N. (2014), "Performance of tunnel lining materials under internal blast loading", *Int. J. Protect. Struct.*, **5**(1), 83-96.

- Choi, S., Wang, J., Munfakh, G. and Dwyre, E. (2006), "3D nonlinear blast model analysis for underground structures", *Proceedings of GeoCongress, ASCE*, New York, NY, USA, February, pp. 1-6.
- Chou, H.S., Yang, C.Y., Hsieh, B.J. and Chang, S.S. (2001), "A study of liquefaction related damages on shield tunnels", *Tunn. Undergr. Space Technol.*, **16**(3), 185-193.
- Davis, J.R. (1996) *Cast Irons*, ASM International, Materials Park, OH, USA.
- De, A. (2012), "Numerical simulation of surface explosions over dry, cohesionless soil", *Comput. Geotech.*, **43**, 72-79.
- Desai, C.S., Zaman, M.M., Lightner, J.G. and Siriwardane, H.J. (1984), "Thin-layer element for interface and joints", *Int. J. Numer. Anal. Meth. Geomech.*, **8**(1), 19-43.
- Farr, J.V. (1990), "One-dimensional loading-rate effects", *J. Geotech. Eng., ASCE*, **116**(1), 119-135.
- Feldgun, V.R., Kochetkov, A.V., Karinska, Y.S. and Yankelevsky, D.S. (2008), "Blast response of a lined cavity in a porous saturated soil", *Int. J. Impact Eng.*, **35**(3), 953-966.
- Fragaszy, R.J. and Voss, M.E. (1986), "Undrained compression behavior of sand", *J. Geotech. Eng., ASCE*, **112** (3), 334-347.
- Han, Y. and Liu, H. (2015), "Finite Element simulation of medium-range blast loading using LS-DYNA", *Shock Vib.*, Article ID 631493.
- He, W., Chen, J.Y. and Guo, J. (2011), "Dynamic analysis of subway station subjected to internal blast loading", *J. Central South Univ. Technol.*, **18**(3), 917-924.
- Jayasinghe, L.B., Thambiratnam, D.P., Perera, N. and Jayasooriya, J.H.A.R. (2013), "Computer simulation of underground blast response of pile in saturated soil", *Comput. Struct.*, **120**, 86-95.
- Jayasinghe, L.B., Thambiratnam, D.P., Perera, N. and Jayasooriya, J.H.A.R. (2014), "Blast response of reinforced concrete pile using fully coupled computer simulation techniques", *Comput. Struct.*, **135**, 40-49.
- Koneshwaran, S., Thambiratnam, D. and Gallage, C. (2015), "Performance of buried tunnels subjected to surface blast incorporating fluid-structure interaction", *J. Perform. Constr. Facil., ASCE*, **29**(3), 04014084.
- Lewis, B.A. (2004), Manual for LS-DYNA Soil Material Model 147; Technical Publication No. FHWA-HRT-04-095, Federal Highway Administration, Washington D.C., USA
- Liu, H. (2009), "Dynamic analysis of subway structures under blast loading", *Geotech. Geol. Eng.*, **27**(6), 699-711.
- Liu, H. (2012), "Soil-structure interaction and failure of cast-iron subway tunnels subjected to medium internal blast loading", *J. Perform. Construct. Facil., ASCE*, **26**(5), 691-701.
- Liu, H. and Nezili, S. (2016), "Centrifuge modeling of underground tunnel in saturated soil subjected to internal blast loading", *J. Perform. Constr. Facil., ASCE*, **30**, 06015001.
- Liu, H. and Song, E. (2006), "Working mechanism of cutoff walls in reducing uplift of large underground structures induced by soil liquefaction", *Comput. Geotech.*, **33**(4-5), 209-221.
- LS-DYNA (2012a), Version 971 R6.0.0 Keyword User's Manual; Livermore Software Technology Corporation (LSTC), CA, USA
- LS-DYNA (2012b), Version 971 R6.0.0 Theory Manual; Livermore Software Technology Corporation (LSTC), CA, USA.
- Lu, Y., Wang, Z. and Chong, K. (2005), "A comparative study of buried structure in soil subjected to blast load using 2D and 3D numerical simulations", *Soil Dyn. Earthq. Eng.*, **25**(4), 275-288.
- UFC 3-340-02 (2008), Structures to Resist the Effects of Accidental Explosions; Department of the Army and Defense Special Weapons Agency, Washington D.C., USA.
- Veyera, G.E. and Charlie, W.A. (1990), "Laboratory study of compressional liquefaction", *J. Geotech. Eng., ASCE*, **116**(5), 790-804.
- Wang, Z., Lu, Y. and Bai, C. (2008), "Numerical analysis of blast-induced liquefaction of soil", *Comput. Geotech.*, **35**(2), 196-209.
- Xu, T.H. and Zhang, L.M. (2015), "Numerical implementation of a bounding surface plasticity model for sand under high strain-rate loadings in LS-DYNA", *Comput. Geotech.*, **66**, 203-218.